Quantifying cell adhesion dynamics using a custom-made fluid shear device: experiments and model

R. Maan G. I. Menon P. A. Pullarkat

Abstract

Cell adhesion plays a crucial role in situations as diverse as stress generation, cell migration and cancer metastasis. The strengths with which cells attach to substrates can be measured by applying forces that are large enough to detach them. Such forces can be applied by shearing the ambient fluid, so that controllable shear stresses are exerted across cells placed within the flow. Here, we report on the design, construction and benchmarking of a compact, inexpensive and efficient shearing device, based on the principle of a cone-plate rheometer, for the measurement of cell adhesion strengths and for the study of cytoskeletal re-organization in response to a shear stress. The device can be easily integrated with in-situ imaging and measurement techniques such as total internal reflection microscopy or confocal microscopy. It can also be combined with variable substrate structures, such as those produced by micro-patterning. We present experimental results as well as a model framework within which the experimental results can be understood theoretically, summarised in analytic expressions for the number of detached cells as a function of shear stress upon ramping of the stress. These provide reasonable estimates for the strength of the focal adhesion complexes that control cell adhesion.

Key words: cell shearing; mechanobiology; adhesion strength; deadhesion dynamics; cell detachment model; shear device

Introduction

Cells that adhere to substrates provide a convenient model system to explore the magnitude and distribution of the forces that cells exert on the extracellular matrix (ECM). The adhesions that cells form with the ECM are mediated principally by a class of adhesion molecules called integrins. In their bound state with ECM receptors, a number of other proteins bind to integrins, forming a complex structure called a focal adhesion. Such focal adhesions (FAs) contain a large number of transmembrane and cytosolic proteins with force-sensitive components, such as talin and vinculin (1–3), making them sensitive mechanosensors (4, 5). Focal adhesions are also dynamic entities, which respond to external stimuli via mechano-chemical feedback processes. By linking the actin cytoskeleton and the ECM, focal adhesions can function both as force and biochemical sensors, linking mechanosensing with downstream signalling cascades that enable cells to modify their behaviour in response to perturbations.

Cell migration, proliferation (6), differentiation (7, 8) and cellular metastasis (9, 10) are all cellular processes that involve the modulation of cell adhesion(11, 12). Changes in cell adhesion are also seen in certain disease states. Adhesion complexes are known to be modified in cancer cells (13) which have been shown to have a higher spread area, to apply large traction forces on their surroundings (14, 15), and to proliferate faster (16). Cells which detach from tumors and metastasize appear to have enhanced focal adhesion dynamics (17), raising questions of how the modification of cell adhesion in disease might lead to impaired force sensing, with downstream consequences for tumour spreading. Such observations also suggest that quantifying variations in the adhesion of cells cultured on substrates might provide interesting insights into this problem.

Investigating cell adhesion at a quantitative level is difficult because adhesions are dynamic and heterogeneous in their sizes and spatial distribution. As a result, depending on the length scale of interest and the questions at hand, several distinct approaches have been used to probe cell-substrate interactions. At a molecular level, atomic force microscopy has been used to study the attachment and detachment dynamics of single bonds (18). Micron sized beads coated with extracellular matrix proteins can be attached to cells and pulled using an AFM or a magnetic tweezers (19). At the single cell level, cell detachment can be studied using micropipettes (20, 21). Finally, population-averaged cell-detachment kinetics can be studied using an external fluid shear stress applied by means of a spinning disc (22, 23) or by using microfluidic flow channels (24). Centrifugation forces have also been

used to study cell detachment (25). Population studies conducted using fluid flow stress or centrifugation are of special importance when comparing differences in gross adhesiveness between cell types. Such population-based methods provide powerful tools to compare normal cells with cells with specific knock-down or knock-out modifications to the focal assembly. From a bio-medical point of view these techniques have the potential to investigate changes in adhesion brought about by metastasis (26). Quantifying cell-substrate adhesion is also essential for the design of compatible synthetic implants (25). Some of the techniques mentioned above have been reviewed recently (27).

If the anomalous behaviour exhibited by cells with compromised adhesion are associated to extreme values of a distribution (28), it is unlikely that assays based on single cells will be sensitive to them. On the other hand, population studies, if based on a sufficiently large population, are likely to accommodate a range of varied cell adhesions, including these extreme ones. Additionally, collective phenomena such as wound healing and metastasis are examples where population studies are more appropriate than single cell studies. Another advantage of population-based studies is that they connect more effectively with theoretical models based on positing a distribution of adhesion strengths and number of focal adhesions. Data testing these models is most efficiently accumulated through population studies rather than through single-cell studies.

A controllable way of measuring the distributions of adhesion strength is to subject adhered cells to fluid shear(29). The most common ways of applying the fluid shear to study the cell detachment kinetics are by means of a spinning disc apparatus (22, 30) or through the use of microfluidic flow channels (24). However, extracting cell adhesion parameters from such measurements requires the development of theoretical models. A theoretical model for the effects of a shear flow on adherent cells must account for the following: Forces acting on the cell arising from the shear flow must be computed accurately - these will depend on cell geometry as well as its modulation by the applied force. Next, the effects of these forces as they act on cell-substrate attachment points must be computed. A probabilistic model for the distribution of attachment points is essential for the understanding of results from population-based studies of cell detachment under an applied force. Finally, the stochastic dynamics of the attachment and de-attachment of individual focal adhesions under external forces must be accounted for. Despite the complexity of this problem, one might hope that simplified models, incorporating what one believes to be essential ingredients, might provide useful insights (31).

Here we discuss a compact, microscope-mountable, home-developed shear device which is cost-effective and compatible with high resolution imaging using any standard TIRF, epi-fluorescence, confocal, or super-resolution microscopy. It can be operated in two distinct modes of operation–constant shear stress or time varying shear stress–to yield measures of cell adhesiveness averaged over a large number of cells. We present a theoretical model for how cell adhesion is modulated under an applied force and extract adhesion parameters from the experiments. We use a load-sharing assumption for the action of these forces on a prescribed number of adhesion points and a generalization, based on a stochastic version of the Bell model, for how de-adhesion occurs at fixed shear stress. Our model considers various forms for the distribution of cell sizes, relating them to the distribution of attachment points. We use these results to arrive at analytic forms for the fraction of cells adhered, upon a fast ramp of the applied shear rate, as well as a formula for the decay of the number of adhered cells with time at an intermediate value of the shear rate. These analytic forms directly derive from the assumptions made for the distribution of cell sizes, as well as for the distribution of the number of attachment points at given spread cell radius, but can be generalized to arbitrary distributions.

Our fits to the functional forms we propose show a good agreement with the experimental data. We demonstrate the usefulness of this device in probing cell adhesion as well as its utility, coupled to the model description, in extracting numerical values of relevant biophysical parameters from population-based assays.

Materials and Methods

Cell Culture

3T3 fibroblast and HEK293T cells were grown on plastic petri dishes coated with fibronectin. The coating was done by exposing the surface to 30 μg/ml fibronectin (Sigma Aldrich) in HBSS for 30 min. The cells were grown in DMEM containing 10% FBS and 1% PSG to about 50% confluency so that they do not touch each other. All reagents were purchased from Invitrogen. After plating, the cells were incubated overnight in 5% CO_2 at 37 °C before experiments.

Imaging and Analysis

In order to quantify the number of cells detached as a function of time and shear stress under fluid shear, we counted labelled nuclei. The cell nuclei were labelled using Hoechst H33342 (Molecular Probes) at 1:1000 ratio of the 10 mg/ml slock solution. The fluorescence imaging was done using a motorized Zeiss AxioObserver-Z1 microscope, an Axiocam CCD camera, and the AxioVision 4.8 software, all supplied by Zeiss. The counting of labelled nuclei was done using in-house MATLAB code that involved counting of bright objects of a specified size range. Another in-house code was written in MATLAB to measure cell areas.

Device Design & fabrication

Our custom-built shear device uses the standard cone and plate geometry to apply controlled fluid shear stress to adherent cells. This custom device is compact and inexpensive and can be mounted on any standard inverted microscope and imaging can be performed in phase contrast, fluorescence, confocal mode etc. for enabling high resolution imaging. A schematic and a photograph of the device are shown in Figs. 1 a,b. A computer hard disk motor removed from a SATA, 3.5", 7200 rpm PC hard disk drives a vertically mounted cone plate at a desired rpm. This precision motor is almost perfectly wobble free and allows for precision coupling of the cone plate with excellent matching of the motor and cone axes. The 1° cone plate and shaft are fabricated out of a single aluminium piece and the cone surface is polished for smoothness. The rpm of the three phase, out-runner, brushless motor is controlled via an electronic speed controller (ESC) (HobbyWing 80020591) which in turn is controlled using pulse width modulation signals from a function generator (Agilent Technologies, 33220A). The actual rpm depends on the load on the motor, which varies with the experimental condition. To measure the actual rpm, the shaft of the cone is painted black except for a thin reflective strip. An encoder unit consisting of an IR LED and a sensor (TCRT5000 reflective sensor module) measures the reflected light pulses and records the rpm on a computer using an Arduino Uno USB I/O board.

The petri dish containing adherent cells is placed below the cone plate and its temperature is controlled using heating foils (Minco) attached to the bottom aluminium base plate and controlled using an calibrated Pt-100 RTD and a temperature controller (CT325 Minco). Three micrometer levelling screws (Thorlabs Inc., KS1, Precision Kinematic Mirror Mount) on the

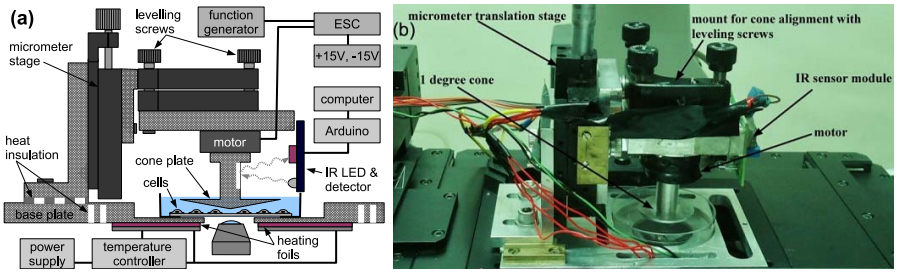

Figure 1: (a) A schematic of the shear device fabricated using a hard disk motor. The rpm of the motor is controlled using an electronic speed controller and a function generator. The rpm is measured using an IR LED and sensor coupled to a computer via an Arduino board. The temperature of the petri dish containing cells is controlled using an electrical temperature controller. The cone is aligned with respect to the petri dish containing the cell monolayer using three micrometer levelling screws. The cone to plate gap is adjusted using a vertical micrometer translation stage. The gap and tilt measurements were performed using encoders on a motorized microscope. Imaging is done in fluorescence mode. (b) A photograph of the shear device mounted on the microscope, with labels indicating the main components. The heating elements attached to the base plate are not visible.

motor mount allows for setting the rotation axis of the cone normal to the surface containing the cells. This alignment is done iteratively by measuring the gap between the bottom flat surface and the top cone plate at three points equidistant from the cone apex. The distance and gap measurements are performed with a resolution better than a micrometer using the motorized XYZ units (with encoders of the Zeiss AxioObserver Z1 microscope), and a long distance 40× objective. The final gap is set by first lowering the cone using the vertical micrometer stage (Thorlabs Inc., MT1, Travel Translation Stage, least count 10μm) till its apex gently presses on the cells below and this point is set as zero. The cone plate is then raised to the desired working distance. The imaging for cell counting was done using a 10× objective.

Results and Discussion

Cell detachment assays

We use two protocols to study the detachment kinetics of adhered cells. In the first, a constant fluid shear stress is applied and the number of cells detached was recorded as a function of time. In the second, the imposed shear stress is increased in steps with a fixed waiting time between steps, with the number of remaining cells counted at the end of each wait time. Our results, obtained using fibroblasts and HEK as model systems, are shown in Fig. 2. The constant shear used in the first protocol and the waiting time

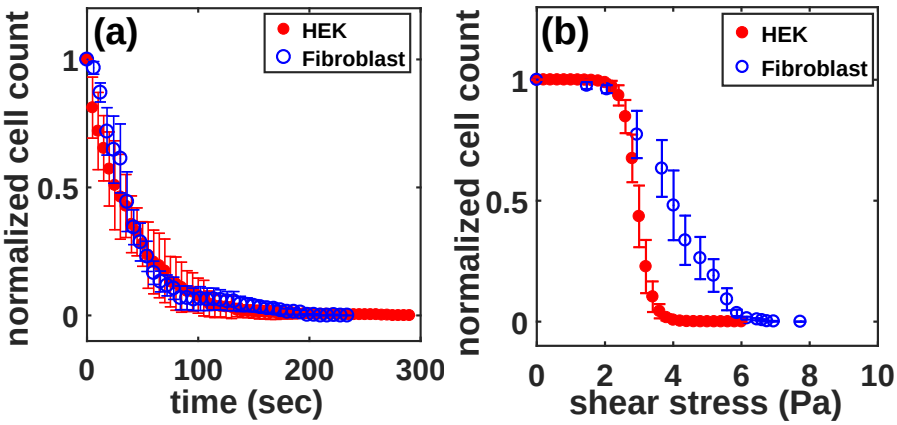

Figure 2: a) Detachment kinetics at a constant fluid shear stress. The value of the shear stress was taken to be that corresponding to the value at which 50% of cells had detached in each case, as extracted from (b), (b) Detachment curves for HEK and fibroblast cell as a function of shear stress with a waiting time of 1 min at every shear value. The curves shown in both (a) and (b) represent an average detachment trend, taken over 4 independent runs. The starting cell count in both cases, for both the cell types, was around 100. Error bars are ± standard deviation (SD).

in the second protocol were decided from prior trials such that the constant shear stress is set to equal the threshold stress seen in Fig. 2b where 50% of the cells are detached. The wait time is chosen to be of the order of the characteristic detachment time obtained in constant stress experiments as the one shown in Fig. 2a. Similar detachment curves have been reported earlier but the quantification we report here is novel(32–34). The number

of attached cells as a function of increasing shear clearly shows an initial plateau where cells do not detach over the times spent at each stress value, since the shear stress is much less than the threshold stress defined by the mid-point of the curves in Fig. 2b.

The number of cells that remain adhered as a function of time at a constant shear stress appears to decay largely as an exponential, although there is a small but significant deviation from this form in the tail region for the 3T3 fibroblast cells. This is possibly due to a small population of well-spread cells of much larger-than-average area in the case of the fibroblast cells, as can be seen in Fig. 3. Note that the 3T3 cells have an average spread area of 1800 μm^2 whereas the HEK cells we used have a significantly lower spread area of 369 μm^2 as shown in Fig. 3. This figure also exhibits numerical fits to the areal distribution for both HEK and fibroblasts in terms of a log-normal distribution, as discussed further below. A theoretical

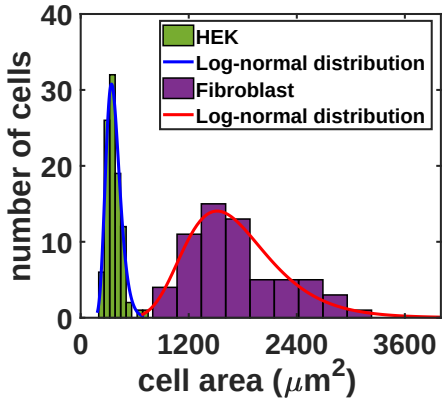

Figure 3: Cell spread area distributions measured for 3T3 fibroblasts and HEK cells as indicated in the figure legend. These indicate that the broader detachment curves in the case of the fibroblasts likely originates in the overall broader distribution of cell sizes. The solid curves in both cases are fits to a log-normal distribution. The parameters that fit the distribution in each case are: $\mu = 5.88, s = 0.22$ (Fibroblast) and $\mu = 7.41, s = 0.299$ (HEK) where μ, s are the mean and standard deviation. The total numbers of cells taken for the distributions are 64 for 3T3 and 100 for HEK.

explanation of the dependence of detachment curves upon the distribution of spread areas of cells is provided in the following section.

Theoretical Model

To estimate the scale of forces exerted on adherent cells in a shear flow, we use results from Price, Pozrikidis and other workers(35–40). Consider shear stresses acting across a solid hemisphere attached to a flat substrate. We assume that the flow is governed by the linear Stokes equation, and is constrained by incompressibility(41, 42). For such a shear flow, with the velocity in the x-direction and the gradient in the z-direction, with shear rate k and fluid dynamical viscosity η and thus wall-shear stress $\sigma = \eta k$, the total force exerted on the hemisphere is $\vec{F} = 13.508\ \sigma R^2 \hat{x}$ where R the cell radius(36). We ignore effects due to the torque since cells in shear flow are observed to be relatively unaffected by lift effects as well as confinement effects which would correct the coefficient above. Taking $R \sim 20\mu m$ ($R_{HEK} \simeq 11\mu m, R_{3T3} \simeq 24\mu m$) and values of σ of around $3.5Pa$ ($\sigma_c \simeq 3Pa$ for HEK cells and $\sigma_c \simeq 4Pa$ for 3T3 cells) required for detachment, we get a force-scale of $\sim 19\ nN$, in the right range as compared to typical experimental values for the total force required for cell detachment(24, 31, 41, 43–45). Estimating the number of adhesion complexes to be around 40, this implies that each adhesion complex exerts approximately 475 pN of force on the substrate, a figure in the appropriate range *vis a vis.* experiments(43). Modelling adherent cultured cells as hemispheres attached to a rigid substrate ignores some important aspects of their geometry. In interphase, such cells are typically well-spread on substrates, with their maximal heights h typically smaller than the spread radii R. The maximal height is controlled by the placement and size of the nucleus and the structure of the F-actin cortical layer (46). Pozrikidis provides numerical solutions for a family of protuberances involving sections of oblate spheroids and semi-spheroids, finding that the scaling of total force with the contact area remains quadratic, although it is modified by a geometric factor which is in the range of about (1-14), with the largest value corresponding to the adhered hemisphere(35, 47).

Here, we have simply equated the forces exerted on the cell by the flow to the cell adhesion forces, ignoring the dynamics of attachment and detachment of adhesion molecules. However, cell adhesion is a collective phenomenon. A mean-field approach to understanding the unbinding and rebinding of adhesion molecules under force F follows from the work of Bell, who considered an adhesion cluster as a set of N molecules capable of binding as well as detaching from a substrate (48). At time t, $N(t)$ are bound while the remaining $N - N(t)$ adhesion molecules are unbound. Each bond breaks with a rate k_{off} and can rebind with a rate k_{on}. The incorporation of a force promotes unbinding via $k_{off} = k_0 \exp\left(F x_b / k_B T N(t)\right) = k_0 \exp\left(F/F_b\right)$

where x_b is a typical bond length scale, T is the temperature, k_B the Boltzmann constant and F_b is a molecular scale force. From the discussion above we can assume that $F_b \simeq 0.5nN$. It is conventional to assume that the load is equally shared by the bound adhesion molecules. These approximations then lead to the mean-field equation for $N(t)$,

$$\frac{dN(t)}{dt} = -N(t)k_0 \exp(Fx_b/k_BTN(t)) + k_{on}(N - N(t)) \tag{1}$$

This is simplified by introducing a dimensionless time $\tau = k_0 t$, rescaling force as $f = F/F_b$, scaling the rebinding rate so that $\gamma = k_{on}/k_0$ and by assuming that a constant force is applied and shared equally between all adhesion molecules. In steady state, this yields $N(\tau)\exp(f/N(\tau)) = \gamma(N - N(\tau))$, an equation which predicts a saddle node bifurcation when $f_c = Np\ln(\gamma/e)$, where the product logarithm is defined as $p\ln(a)$ from the solution of $x \exp x = a$. This implies that adhesion is stable up to a critical force f_c in mean-field theory(31, 49, 50).

Such a mean-field description ignores fluctuations. Stochasticity can be incorporated in terms of a one-step master equation for the quantity p_i, where p_i is the probability of having i adhesion molecules bound at time t(31, 49–52). Such an equation incorporates both loss and gain terms and can be written as

$$\frac{dp_i}{dt} = r(i+1)p_{i+1} + g(i-1)p_{i-1} - [r(i) + g(i)]p_i. \tag{2}$$

With rates appropriate for the Bell model with load sharing $r(i) = i\exp(f/i)$ and $g(i) = \gamma(N - i)$, the mean first passage time T can then be obtained from a result of Van Kampen(31, 49). This result yields a logarithmic dependence of T on the force for small forces and an exponential dependence at large forces, with the cross-over defining a characteristic (dimensionless) force value f_c. Note that adhesion involving an finite number of adhesion molecules, each with a characteristic unbinding force, must ultimately be unstable, although the characteristic time for detachment can be large, depending on N. This treatment also suggests two experimentally relevant regimes, the first in which the mean number of attachment points is instantly equilibrated as the shear stress is ramped in steps but any further fluctuations are ignored. This is essentially a short-time or fast-loading approximation. A second limit is one in which we wait at each imposed shear stress value for times comparable to the first passage time T, in which case we must account for the dynamics of detachment in detail.

We draw intuition from kinetic Monte Carlo methods that incorporate stochasticity to compute the fraction of bound cells at time t following the

application of the flow, in the short-time limit described above. We simulate directly the stochastic process defined by the equations above using the Gillespie method (53–55). We determine the average fraction of cells which are adhered at a particular level of shear, given that they are observed *up to* a given time t_0, as measured from the initiation of the shear flow. Our calculations first assume a fixed initial number of adhesion molecules $(50 - 100)$, simulated using Eq. 2. Our choice of rates follows that of the Bell model. Our results are shown in Fig. 4(a). where we have varied

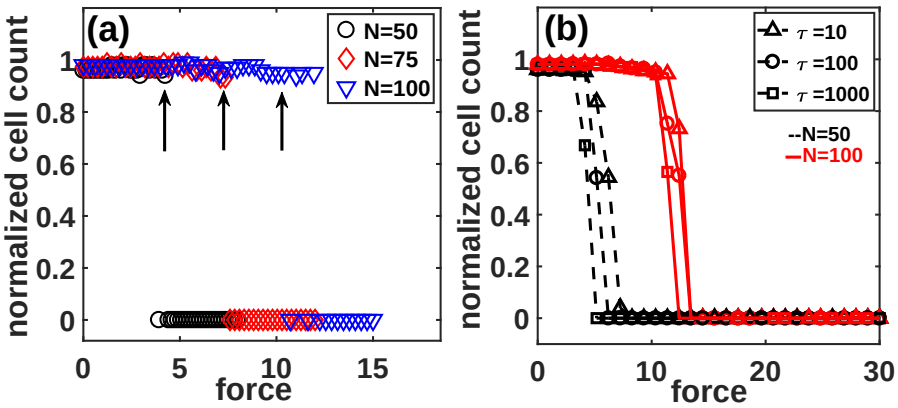

Figure 4: (a) Fraction of adhered cells as a function of force acting on the adhered cell via a shear flow, as computed using kinetic Monte Carlo methods as appropriate to the Bell model. This is shown for three values of N, the steady state number of attachment points at small times in the absence of a force. Note the sharp drop in this fraction near a critical force f_c (vertical arrows) which scales linearly with the number of initial attachment points. All cells are assumed to be identical in size. (b) Fraction of adhered cells as a function of applied force. Each set of curves for a given N (given color) are for different waiting time (different symbols) at each force value varied over a logarithmic scale. As the waiting time is increased, the threshold value decreases, while the essentially sharp decrease of this fraction at the waiting time and N-dependent threshold value remains a feature of the data.

N, the mean number of attachment points at zero force. Note that there is an essentially sharp transition between a state in which the number of attachment points varies from a value close to N to zero. The force value at which this transition occurs is subject to hysteresis between different runs,

but the values cluster about a mean detachment force that scales linearly with N, as in the simple Bell model. Fig. 4(b) shows that as the waiting time at each force value increases, the threshold value decreases, leaving intact the step jump of this fraction at a waiting-time-dependent critical force. The systematic decrease of the threshold with increasing waiting time also reflects the fact that cell detachment in the presence of stochastic fluctuations involves a barrier crossing process. We model the experimental data by using the result that the critical force for the abrupt detachment of a cell with N equivalent attachment points increases linearly with N, $F_c(N) = \alpha N$.

We can relate the applied shear stress σ to the total force F experienced by each cell, which will, in general, depend on the shape of the cell and the characteristic length-scales over which the flow is perturbed. Our basic question relates to the fraction of adhered cells $\Phi(\sigma)$ that are observed to survive when the shear stress is increased to σ from zero. $\Phi(\sigma)$ will depend on the history of the shear, both if we assume that detached cells are lost via flow outside the imaging region as well as if we take into account the stochasticity in the detachment and attachment of focal adhesions.

For concreteness, we will consider the case where the shear stress is ramped up fast from zero, essentially ensuring that only those cells which are absolutely unstable to detachment are removed, returning later to the case in which we wait at each stress value for a defined time, as in the experiments. The derivative

$$P(\sigma) = -\frac{d\Phi(\sigma)}{d\sigma} \tag{3}$$

represents the fraction of cells that detach between σ and $\sigma + d\sigma$. Thus, we have

$$\Phi(\sigma) = 1 - \int_0^\sigma d\sigma' \; P(\sigma'). \tag{4}$$

We wish to calculate $P(\sigma)$ for a set of adhered cells with the quantities R and N given by a joint distribution $P(N, R)$. This is given by

$$P(\sigma) = \langle \delta(\sigma - \sigma_\sigma^c(N, R)) \rangle, \tag{5}$$

where the averages, denoted by $\langle \cdot \rangle$, are over the probability distribution $P(N, R)$. The shear stress σ is related to the force exerted on the cell by the flow and the critical value of the shear stress is denoted by $\sigma_\sigma^c(N, R)$. Thus,

$$P(\sigma) = \langle \delta(\sigma - \sigma_c(N, R)) \rangle = \int dN \int dR \; \delta(\sigma - \sigma_\sigma^c(N, R)) P(N, R) \tag{6}$$

Now, we can decompose this joint probability in terms of the conditional probabilities

$$P(N, R) = P(N|R)P(R) \tag{7}$$

We will make the approximation that the conditional probability of having N attachment points is slaved to the radius R and has a particularly simple form,

$$P(N|R) = \delta(N - \alpha R^a). \tag{8}$$

The distribution of cell sizes then determines $P(\sigma)$ completely. Then, the probability distribution of critical depinning forces given a probability distribution of R is

$$P(\sigma) = \int dR\ \delta(\sigma - \sigma_c(\alpha R^a, R))P(R) = \int dR\ P(\sigma|R)P(R). \tag{9}$$

The shear force experienced by our model cell is $F_{shear} = \mathcal{C}\dot{\gamma}\eta R^2 = \sigma\mathcal{C}R^2$, with $\mathcal{C}$ a geometric factor reflecting the aspect ratio of the adhered cell, η is the viscosity, σ the wall stress and R the radius of the circular section in contact with the substrate. This force is opposed by forces from the FA's: $F_{adhesions} = Nf = \alpha R^a f$, where we have assumed that the number N of focal adhesions is directly proportional to R raised to an appropriate power and the magnitude and dimensions of α defined accordingly. If FA's are distributed largely along the perimeter, then $a = 1$, which is the limit we consider. Equating these, we obtain $\mathcal{C}\dot{\gamma}_c\eta R^2 = \sigma_c\mathcal{C}R^2 = \alpha R^a f$, which provides an estimate for the critical shear stress defined through

$$\sigma_c = \frac{\alpha R^{a-2} f}{\mathcal{C}}. \tag{10}$$

When $a = 1$, corresponding to FA's concentrated along the perimeter of the cell, we have

$$\sigma_c = \frac{\alpha f}{\mathcal{C}R} = \frac{D}{R}, \tag{11}$$

where $D = \alpha f/\mathcal{C}$.

Assuming that the distribution of spread cell sizes is log-normal(56), we have

$$P(R) = \frac{1}{Rs\sqrt{2\pi}} e^{-(\ln R - \mu)^2/2s^2}, \tag{12}$$

where μ and s are the location and scale parameters of the associated normal distribution. Given

$$P(\sigma|R) = \delta(\sigma - D/R), \tag{13}$$

we obtain

$$P(\sigma) = \frac{1}{\sigma s\sqrt{2\pi}} e^{-(\ln(D/\sigma)-\mu)^2/2s^2} = \frac{1}{\sigma s\sqrt{2\pi}} e^{-(\ln(D/\sigma)-\ln(D/\sigma_0))^2/2s^2}, \quad (14)$$

with

$$\mu = \ln(D/\sigma_0), \quad (15)$$

which we simplify as

$$P(\sigma) = \frac{1}{\sigma s\sqrt{2\pi}} e^{-(\ln(\sigma/\sigma_0))^2/2s^2}. \quad (16)$$

Now we have

$$\Phi(\sigma) = 1 - \frac{1}{s\sqrt{2\pi}} \int_0^\sigma d\sigma' \, \frac{1}{\sigma'} \, e^{-(\ln(\sigma'/\sigma_0))^2/2s^2}. \quad (17)$$

Using the definition of the error function

$$\mathrm{erf}(x) = \frac{2}{\sqrt{\pi}} \int_0^x e^{-t^2} dt, \quad (18)$$

this finally yields

$$\Phi(\sigma) = \frac{1}{2}\left[1 - \mathrm{erf}(\frac{\ln(\sigma/\sigma_0)}{\sqrt{2}s})\right]. \quad (19)$$

When $\sigma = \sigma_0$, $\Phi(\sigma) = 1/2$, defining the critical force σ_0 as the point where half of the cells have detached upon a fast ramp.

This expression, Eqn. 19, contains fit parameters σ_0 and s. The first of these, σ_0, can be directly inferred from data, since it is just the value at which half of the cells have detached. We optimise the value of s to obtain the best fits. In Fig. 5 we show the experimental data of Fig 2 against our prediction of Eqn. 19. For the data shown in Fig. 5(a), these parameters are: $\sigma_0 = 2.91, \sqrt{2}s = 0.18$ (HEK) and in Fig. 5(b) $\sigma_0 = 3.85, \sqrt{2}s = 0.35$ (Fibroblasts). The quantity s is proportional to the width of the distribution of the number of attachment points across cells, which we assume is equivalent to the distribution of cell radii. We have also implicitly assumed that all adhesion points are alike.

To understand the behaviour in the limit that we spend a sufficiently long time at each force value, we must take into account the dynamics of the adhesion molecules, in particular the fact that fluctuations can carry an otherwise stable cluster of attachment points to a regime where adhesion becomes unstable. It is simplest to assume that σ_0 as a function of time

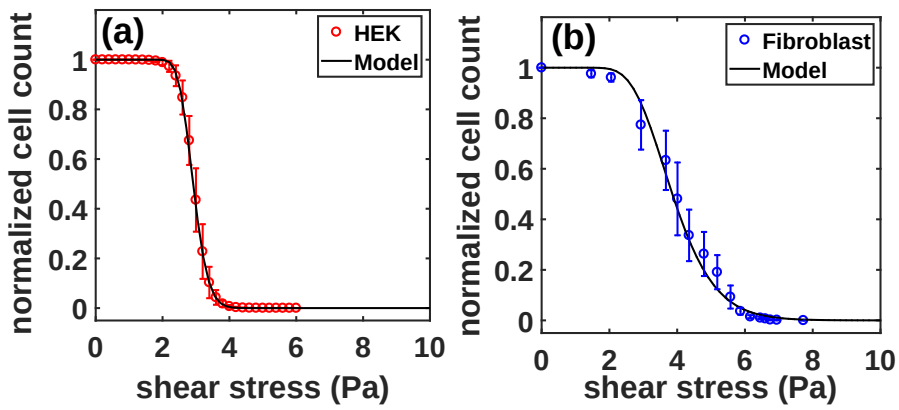

Figure 5: (a) Plot of the experimental data for HEK cells shown in Fig 2 against the model prediction of Eq. 19 with the values of σ_0 and s obtained from a best-fit analysis and (b) Plot of the experimental data for fibroblast cells as shown in Fig 2 against the model prediction of Eq. 19 with the values of σ_0 and s obtained from a best-fit analysis.

decays as an exponential with a characteristic time scale τ, since this is consistent with the absence of a force dependence of the first passage time in this limit. We thus have,

$$\sigma_0(t) = \sigma_0 e^{-t/\tau}. \tag{20}$$

This then yields,

$$\Phi(\sigma, t) = \frac{1}{2}\left[1 - \mathrm{erf}(\frac{\ln(\sigma e^{t/\tau}/\sigma_0)}{\sqrt{2}s})\right]. \tag{21}$$

One further simplification is obtained when $\sigma = \sigma_0$, *i.e.* we examine relaxation at the value of the shear stress where 50% of cells are unstable to detachment upon a fast ramp. In this limit, and normalizing to the number of cells present at $t = 0$, we have,

$$\Phi(\sigma_0, t) = \left[1 - \mathrm{erf}(\frac{1}{\sqrt{2}s}\frac{t}{\tau})\right]. \tag{22}$$

In Fig. 6 we show the data for both HEK and fibroblasts, where the fit form is obtained by using the values of $\sqrt{2}s$ from the prior fits for the separate cases of HEK and fibroblasts and the value of τ is changed till an

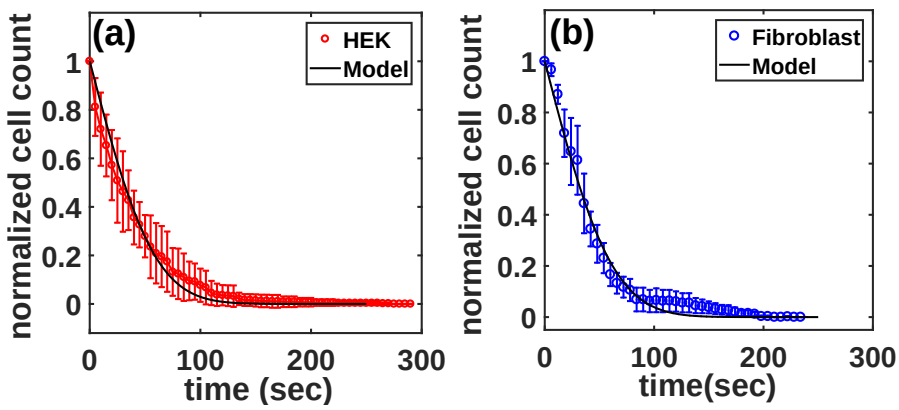

Figure 6: (a) Plot of the fitting function $\Phi(\sigma_0, t) = \left[1 - \mathrm{erf}(\frac{1}{\sqrt{2}s}\frac{t}{\tau})\right]$ against the experimental data for detachment as a function of time at fixed stress σ_0 for HEK cells, (b) Plot of the fitting function $\Phi(\sigma_0, t) = \left[1 - \mathrm{erf}(\frac{1}{\sqrt{2}s}\frac{t}{\tau})\right]$ against the experimental data for detachment as a function of time at fixed stress σ_0 for fibroblasts. In both cases, we take the values of σ_0 to be the midpoint value of the detachment curve, i.e. the value of the stress at which, on a fast ramp, 50% of cells are observed to detach. We take the values of s from fits to the detachment curve, leaving τ as the only undetermined parameter which we optimise to obtain the best fit.

optimum fit is obtained. In this manner we obtain $\tau = 190s$ for fibroblasts and $\tau = 350s$ for HEK cells. These time-scales are perhaps most accurately as averaged first passage times to the detached state, where the average is taken over a distribution of number of attachment points across cells of different spread sizes as well as over a large number of stochastic realisations.

In principle we might have expected, given the theoretical development, that the value of s obtained from fitting the distribution of cell spread areas to a log-normal form should be the one that is used to fit the detachment data, both as a function of increasing shear stress as well as a a function of time at fixed shear stress. In practice, there is a difference between these values: $\sqrt{2}s = 0.31$ for HEK cells as obtained from Fig. 3, whereas $\sqrt{2}s = 0.18$ from the best fit values in Fig. 5. For fibroblasts, the discrepancy is smaller, with $\sqrt{2}s = 0.42$ from the fits in Fig. 3 as against a value of $\sqrt{2}s = 0.35$ from the best fit values in Fig. 5. This relatively minor difference could originate in a number of approximations we have made along the way: First, we have ignored heterogeneities in the number of detachment points

N, assuming that N scales simply with the radius and is uniquely prescribed, once R is supplied. Second, we idealised all cells as characterized by only their spread area, via a single quantity R. Third, we have ignored variations in the strength of different focal adhesions. Given these somewhat stringent approximations, the fact of a minor discrepancy between the theoretical predicted values extracted from the cell-size distribution data and the 'best-fit' values of s extracted from the detachment curves is unsurprising.

Conclusion

This paper has described the development and the benchmarking of a compact and inexpensive cell shearing device for the study of the detachment dynamics of cells under fluid shear stress. It is made of inexpensive components, such as a high precision computer hard-disk motor from a discarded disk controlled by an electronic speed controller and a Arduino board. The micrometer adjustment screws and the heating elements can also be implemented easily using ready made and inexpensive items. The use of a 30mm coverglass as the bottom surface of the petri allows for in-situ high resolution imaging. As it is extremely compact, the device can be easily mounted on any standard inverted microscope. It can thus be used in combination with different types of fluorescence microscopy techniques, such as confocal and total internal reflection (TIRF) microscopy.

Although spinning disk devices have been used in the past to study cell detachment under shear stress there are a few drawbacks which prevent them from being more widely employed. The use of a commercial rheometer as in Derks et al. (57) is attractive due to the ease of use and the range of accessible protocols but such devices are prohibitively expensive if used primarily for cell detachment studies. Shear devices can also be technically challenging to fabricate (58). Several of the reported custom devices are unsuitable for in-situ visualization of cell detachment dynamics and require post-analysis by removing the cell culture plate (23, 59). Microfluidic flow channels such as described in Decave et al., Steward et al., Couzon et al., and Lu et al. (24, 60–62) are compatible with microscopy but achieving high enough flow rates to study cell detachment is difficult. Such devices are often prone to disastrous leaks when used with thin coverglasses (for high resolution) on expensive microscopes. Besides this, even with recirculation, flow technique requires a large amounts of culture medium for long term experiments. This becomes an issue especially when using expensive biochemical reagents (drugs) that perturb cell adhesion properties. A comprehensive review of the

different techniques for the measurement of cell adhesion, describing their relative advantages and applications, can be found in the review by Khalili and Ahmad (27). Our device overcomes some of the difficulties mentioned above. In addition, a significant aspect of the present study is that we have performed de-adhesion experiments in two complementary modes: constant shear stress and time-varying shear stress.

The theoretical model we have developed provide excellent fits to both sets of data using the same parameters. We show that the time varying shear stress mode is better at discerning differences in adhesion of HEK and 3T3 cells. Since, in particular, cancerous cells are known to differ from normal cells in their adhesion strengths, the device can potentially be used to distinguish between such cells using a population-based measurement (26). Our theoretical model incorporates both stochasticity as well as the ability to account for cell size distributions in order to describe the detachment dynamics under the two modes of measurement. The theoretical analysis indicates that even if we assume that all focal adhesions are identical, accounting for variations in cell size and any accompanying variation in the number of attachment points across cells could account quantitatively for the shapes of the detachment curves. This observation suggests that our methodology can be used to distinguish delicate differences in the cell adhesion across different cell lines or cells with different modifications. For the two cell lines we study, these differences can be argued to arise directly from the distribution of cell sizes which is different in both cases. This distribution influences the predicted detachment curves, since it determines the width of the detachment curve.

Our theory accommodates an arbitrary distribution of cell sizes, although for simplicity we confined ourselves to calculations for the log-normal distribution. Importantly, a single set of parameters σ_0 and s, fits both the constant shear stress and time-varying shear stress data. In particular, the quantity s can be interpreted as the width of the distribution of the number of attachment points, which is equivalent (apart from a dimensional multiplicative factor) to the distribution of spread cell radii in the simple model described here. Given the generality of the approach described here, it is easy to accommodate more complex joint distributions $P(R, N)$ as well as to incorporate more detailed biophysical modelling of variations in adhesion strengths.

A further improvement of the setup would involve the use of micropatterned substrates to restrict cells to well defined sizes and shapes. In this case, we can test our assumptions of simple linear relationships between the number of adhesion points, the radius corresponding to the spread area of

the cell and inhomogeneities of the force scale of different attachment points. Working with synchronised cells will reduce one source of uncertainty in the data. Incorporating these modifications to the experiment and analysis should improve our understanding of, as well as our ability to quantitatively describe, the biophysical underpinnings of cell adhesion phenomena.

Acknowledgements

We gratefully acknowledge funding from the PRISM project of the Institute of Mathematical Sciences, Chennai. We are particularly grateful to Namrata Gundiah for useful discussions and Rahul Siddharthan for a productive conversation.

References

[1] Hirata, H., H. Tatsumi, C. T. Lim, and M. Masahiro, 2014. Force dependent vinculin binding to talin in live cells: a crucial step in anchoring the actin cytoskeleton to focal adhesions. *Am J Physiol Cell Physiol* 306:C607–620.

[2] Lee, S. E., R. D. kamm, and M. Mofrad, 2007. Force-induced activation of talin and its possible role in focal adhesion mechanotransduction. *J. Biomech.* 40:2096–106.

[3] Mierke, C. T., 2009. The role of vinculin in the regulation of the mechanical properties of cells. *Cell Biochem. Biophys* 53:115–126.

[4] Geiger, B., J. P. Spatz, and A. D. Bershadsky, 2009. Environmental sensing through focal adhesions. *Nat. Rev. Mol. Cell Biol.* 10:21–33.

[5] Yan, J., M. Yao, B. T. Goult, and M. Sheetz, 2015. Talin dependent Mechanosensitivity of cell focal adhesions. *Cel. Mol. Bioeng.* 8:151.

[6] Stoker, M., C. O'Neill, S. Berryman, and V. Waxman, 1968. Anchorage and growth regulation in normal and virus-transformed cells. *International Journal of Cancer* 3:683–693.

[7] Engler, A. J., S. Sen, H. L. Sweeney, and D. Disher, 2006. Matrix elasticity directs stem cell lineage specification. *Cell* 126:677–689.

[8] Evans, N. D., C. Minelli, E. Gentleman, V. LaPointe, S. N. Patankar, et al., 2009. Substrate Stiffness affects early differentiation events in Embryonic Stem Cells. *Eur Cell mat.* 18:1–14.

[9] Cavallaro, U., and G. Christofori, 2001. Cell adhesion in tumor invasion and metastasis: loss of the glue is not enough. *BBA - Reviews on Cancer* 1552:39 – 45.

[10] Somasiri, A., J. S. Nielsen, N. Makretsov, M. L. McCoy, L. Prentice, C. B. Gilks, S. K. Chia, K. A. Gelmon, D. B. Kershaw, D. G. Huntsman, K. M. McNagny, and C. D. Roskelley, 2004. Overexpression of the Anti-Adhesin Podocalyxin Is an Independent Predictor of Breast Cancer Progression. *Cancer Research* 64:5068–5073.

[11] Elineni, K. K., and N. D. Gallant, 2011. Regulation of cell adhesion strength by peripheral focal adhesion distribution. *Biophysical journal* 101:2903–2911.

[12] Selhuber-Unkel, C., T. Erdmann, M. Lopez-Garcia, H. Kessler, U. Schwarz, and J. P. Spatz, 2010. Cell adhesion strength is controlled by intermolecular spacing of adhesion receptors. *Biophysical Journal* 98:543–551.

[13] Seguin, L., J. S. Desgrosellier, S. M. Weis, and D. A. Cheresh, 2015. Integrins and Cancer: regulators of cancer stemness, metastasis and drug resistance. *Trends in cell Biol.* 25:234–240.

[14] Kraning, C. M., J. P. Califano, and C. Reinhart-King, 2012. Cellular traction stresses increase with increasing metastasis potential. *PLoS One* 7:26770–85.

[15] Indra, I., V. Undyala, C. Kandow, U. Thirumurthi, M. Dembo, and K. A. Beningo, 2011. Am *in vitro* correlation of mechanical forces and metastatic capacity. *Phy. Biol.* 8(1):015015.

[16] Tubiana, M., 1989. Tumor Cell Proliferation Kinetics and Tumor Growth Rate. *Acta Oncologica* 28:113–121.

[17] Bijian, K., C. Lougheed, J. Su, B. Xu, J. H. wu, K. Riccio, and M. A. Alaoui-Jamali, 2013. Targeting focal adhesion turnover in invasive breast cancer cells by the purine derivative reversine. *BJC* 109:2810–2818.

[18] Franz, C. M., A. Taubenberger, P.-H. Puech, and D. J. Muller, 2007. Studying Integrin-Mediated Cell Adhesion at the Single-Molecule Level Using AFM Force Spectroscopy. *Science Signaling* 2007:pl5–pl5.

[19] Diz-Muoz, A., D. A. Fletcher, and O. D. Weiner, 2013. Use the force: membrane tension as an organizer of cell shape and motility. *Trends in Cell Biology* 23:47 – 53.

[20] Puech, P.-H., K. Poole, D. Knebel, and D. J. Muller, 2006. A new technical approach to quantify cellcell adhesion forces by AFM. *Ultramicroscopy* 106:637 – 644.

[21] Salnki, R., C. Hs, N. Orgovan, B. Pter, N. Sndor, Z. Bajtay, A. Erdei, R. Horvath, and B. Szab, 2014. Single Cell Adhesion Assay Using Computer Controlled Micropipette. *PLOS ONE* 9:1–12.

[22] Garcia, A. J., P. Ducheyne, and D. Boettiger, 1997. Quantification of cell adhesion using a spinning disc device and application to surface-reactive materials. *Biomaterials* 18:1091–1098.

[23] Furukawa, K. S., T. Ushida, T. Nagase, H. Nakamigawa, T. Noguchi, T. Tamaki, J. Tanaka, and T. Tateishi, 2001. Quantitative analysis of cell detachment by shear stress. *Materials Science and Engineering: C* 17:55 – 58.

[24] Couzon, C., A. Duperray, and C. Verdier, 2009. Critical stresses for cancer cell detachmnet in microchannels. *Eur Biophys J.* 38(8):1035–47.

[25] Reyes, C. D., and A. J. García, 2003. A centrifugation cell adhesion assay for high-throughput screening of biomeaterial surfaces. *J Biomed Mater Res A.* 67(1):328–33.

[26] Fuhrmann, A., A. Banisadr, P. Beri, T. D. Tlsty, and A. J. Engler, 2017. Metastatic state of cancer cells may be indicated by adhesion strength. *Biophys J.* 112:736–745.

[27] Khalili, A. A., and M. R. Ahmed, 2015. A Review of cell adhesion studies for Biomedical and Biological applications. *Int J Mol Sci* 16:18149–18184.

[28] Irmscher, M., K. V. Laarhoven, A. M. D. Jong, and M. Prins, 2013. The influence of inhomogenous adhesion on the detachmnet dynamics of adhering cells. *Eur Biophys J* 43:419.

[29] Fuhrmann, A., and A. J. Engler, 2015. The cytoskeleton regulates cell attachment strength. *Biophysical journal* 109:57–65.

[30] Fernández, P., L. Heymann, A. Ott, N. Aksel, and P. A. Pullarkat, 2007. Shear rheology of a cell monolayer. *New J. of Phy.* 9:419.

[31] Schwarz, U. S., and S. A. Safran, 2013. Physics of adherent cells. *Reviews of Modern Physics* 85:1327.

[32] Mitchell, J. S., W. S. Brown, D. G. Woodside, P. Vanderslice, and B. W. McIntyre, 2009. Clustering T-cell GM1 lipid rafts increases cellular resistance to shear on fibronectin through changes in integrin affinity and cytoskeletal dynamics. *Immun. and cell Biol.* 87:324–336.

[33] Christophis, C., M. Grunze, and A. Rosenhahn, 2010. Quantification of the adhesion strength of fibroblast cells on ethylene glycol terminated self-assembled monolayers by a microfluidic shear force assay. *Phys. Chem. Chem. Phys.* 12:4498–4504.

[34] Cheung, L. S. L., X. Zheng, A. Stopa, J. C. Baygents, R. Guzman, J. A. Schroeder, R. L. Heimark, and Y. Zohar, 2009. Detachment of captured cancer cells under flow acceleration in a bio-functionalized microchannel. *Lab Chip* 9:1721–1731.

[35] Pozrikidis, C., 1997. Shear flow over a protuberance on a plane wall. *Journal of Engineering Mathematics* 31:29–42.

[36] Price, T., 1985. Slow linear shear flow past a hemispherical bump in a plane wall. *The Quarterly Journal of Mechanics and Applied Mathematics* 38:93–104.

[37] Gaver, D. P., and S. M. Kute, 1998. A theoretical model study of the influence of fluid stresses on a cell adhering to a microchannel wall. *Biophysical journal* 75:721–733.

[38] Sugiyama, K., and M. Sbragaglia, 2008. Linear shear flow past a hemispherical droplet adhering to a solid surface. *Journal of Engineering Mathematics* 62:35–50.

[39] Das, T., T. K. Maiti, and S. Chakraborty, 2008. Traction force microscopy on-chip: shear deformation of fibroblast cells. *Lab on a Chip* 8:1308–1318.

[40] Hammer, D. A., and D. A. Lauffenburger, 1987. A dynamical model for receptor-mediated cell adhesion to surfaces. *Biophysical journal* 52:475–487.

[41] Couzon, C., A. Duperray, and C. Verdier, 2009. Critical stresses for cancer cell detachment in microchannels. *European Biophysics Journal* 38:1035–1047.

[42] Hazel, A., and T. Pedley, 2000. Vascular endothelial cells minimize the total force on their nuclei. *Biophysical Journal* 78:47–54.

[43] Ambrosi, D., A. Duperray, V. Peschetola, and C. Verdier, 2009. Traction patterns of tumor cells. *Journal of mathematical biology* 58:163.

[44] Butler, J. P., I. M. Tolić-Nørrelykke, B. Fabry, and J. J. Fredberg, 2002. Traction fields, moments, and strain energy that cells exert on their surroundings. *American Journal of Physiology-Cell Physiology* 282:C595–C605.

[45] Dembo, M., and Y.-L. Wang, 1999. Stresses at the cell-to-substrate interface during locomotion of fibroblasts. *Biophysical journal* 76:2307–2316.

[46] Vishavkarma, R., S. Raghavan, C. Kuyyamudi, A. Majumder, J. Dhawan, and P. A. Pullarkat, 2014. Role of Actin Filaments in Correlating Nuclear Shape and Cell Spreading. *PLOS ONE* 9:1–13.

[47] Wang, Y., and P. Dimitrakopoulos, 2006. Nature of the hemodynamic forces exerted on vascular endothelial cells or leukocytes adhering to the surface of blood vessels. *Physics of Fluids* 18:087107.

[48] Bell, G. I., et al., 1978. Models for the specific adhesion of cells to cells. *Science* 200:618–627.

[49] Van Kampen, N. G., 1992. Stochastic processes in physics and chemistry, volume 1.

[50] Erdmann, T., and U. Schwarz, 2004. Stability of adhesion clusters under constant force. *Physical review letters* 92:108102.

[51] Seifert, U., 2000. Rupture of multiple parallel molecular bonds under dynamic loading. *Physical Review Letters* 84:2750.

[52] Liang, H.-H., and H.-Y. Chen, 2011. Strength of adhesion clusters under shared linear loading. *Physical Review E* 83:061914.

[53] Gillespie, D. T., et al., 1977. Exact stochastic simulation of coupled chemical reactions. *J. phys. Chem* 81:2340–2361.

[54] Gillespie, D. T., 1976. A general method for numerically simulating the stochastic time evolution of coupled chemical reactions. *Journal of computational physics* 22:403–434.

[55] Schwarz, U. S., T. Erdmann, and I. B. Bischofs, 2006. Focal adhesions as mechanosensors: the two-spring model. *Biosystems* 83:225–232.

[56] Hosoda, K., T. Matsuura, H. Suzuki, and T. Yomo, 2011. Origin of lognormal-like distributions with a common width in a growth and division process. *Physical Review E* 83:031118.

[57] Derks, D., H. Wisman, A. van Blaaderen, and A. Imhof, 2004. Confocal microscopy of colloidal dispersions in shear flow using a counter-rotating coneplate shear cell. *Journal of Physics: Condensed Matter* 16:S3917.

[58] Dieterich, P., M. Odenthal-Schnittler, C. Mrowietz, M. Krmer, L. Sasse, H. Oberleithner, and H.-J. Schnittler, 2000. Quantitative Morphodynamics of Endothelial Cells within Confluent Cultures in Response to Fluid Shear Stress. *Biophysical Journal* 79:1285 – 1297.

[59] Fuhrmann, A., and A. J. Engler, 2015. Acute shear stress direction dictates adherent cell remodeling and verifies shear profile of spinning disk assays. *Physical Biology* 12:016011.

[60] Décavé, E., D. rivier, Y. Bréchet, B. Fourcade, and F. Bruckert, 2002. Shear Flow-Induced Detachment Kinetics of Dictyostelium discoideum Cells from Solid Substrate. *Biophysical Journal* 82:2383 – 2395.

[61] Steward, R., D. Tambe, C. C. Hardin, R. Krishnan, and J. J. Fredberg, 2015. Fluid shear, intercellular stress, and endothelial cell alignment. *American Journal of Physiology - Cell Physiology* 308:C657–C664.

[62] Lu, H., L. Y. Koo, W. M. Wang, D. A. Lauffenburger, L. G. Griffith, and K. F. Jensen, 2004. Microfluidic Shear Devices for Quantitative Analysis of Cell Adhesion. *Analytical Chemistry* 76:5257–5264.